3D PRINTING AND ADDITIVE MANUFACTURING
Volume 11, Number 2, 2024

DOI: 10.1089/3dp.2022.0150

REVIEW ARTICLE

Wire-Arc Additive Manufacturing of Nano-Treated Aluminum Alloy 2024

Yitian Chi,[1] Narayanan Murali,[2] Tianqi Zheng,[1] Jingke Liu,[1] and Xiaochun Li[1,2]

Abstract

With high strength and good fatigue resistance, Al–Cu alloys such as AA2024 are widely used in the aerospace and automotive industries. However, the system's susceptibility to hot cracking and other solidification defects hinders its development in metal additive manufacturing (AM). A nano-treated AA2024 deposition, with the addition of TiC nanoparticles, is successfully additively manufactured without cracks. Microstructural analysis suggests nanoparticles not only mitigate the hot cracking sensitivity but also significantly refine and homogenize grains, resulting in an average size of $23.2 \pm 0.4\,\mu$m. Microhardness profiles show consistent mechanical performance along the build direction, regardless of cyclic thermal exposure. Finally, excellent tensile strength and elongation up to 428 MPa and 7.4% were achieved after heat treatment. The combined results show a great promise of nano-treating in high-strength aluminum AM.

Keywords: additive manufacturing, aluminum alloys, WAAM, nanocomposite

Introduction

In contrast to powder-based metal additive manufacturing (AM), wire-arc additive manufacturing (WAAM), with a lower feedstock material cost and larger build volume, has stood out from other AM technologies in recent years. In addition, a high production rate along with increased design freedom and part complexity make it appealing to the automotive and aerospace industries. High-strength aluminum alloys, such as AA2024, with high strength-to-weight ratios, excellent fatigue resistance, and good corrosion resistance, are extensively used in aerospace applications. However, this alloy's susceptibilities to hot cracking, shrinkage porosity, and macrosegregation[1] result in limited castability, weldability, and printability in metal AM.

To alleviate the alloy's hot cracking sensitivity, three major approaches have been explored in the past. The first is to modify the cooling rate and thermal gradient. Nie et al successfully printed Al–Cu–Mg with optimized process parameters,[2] but despite the reasonable microhardness the deposit achieved, there was no tensile testing study undertaken to fully evaluate its mechanical performance. The second approach is to control the solidification range and melt pool behavior, which also showed promise in mitigating hot cracking issues. The third is to introduce a finer grain structure by providing extra heterogeneous nucleation sites to improve eutectic liquid backfilling and accommodate thermal tensile stresses upon solidification.[3–8] Studies have been conducted by adding Zr[9,10] and Si[11] to current 2xxx aluminum alloy compositions.

The addition of Zr reduces the solidification temperature range, whereas Si can improve the flow behavior of the melt pool; Zr and Si also were also shown to refine the alloy's grain structure. However, even a small amount of Zr could increase the material cost significantly, and no success has been shown in AA2024 WAAM until recently. Nano-treating, modifying an alloy by adding a small fraction of nanoparticles, can control solidification behavior,[12] delay the grain coherency point,[13] and refine grain structures and secondary phases,[6] resulting in the elimination of hot cracking during solidification. Besides, previous studies also established the effects of nano-treating on the electrical conductivity,[14] thermal conductance,[15] and tribological behaviors.[16]

In this study, we use WAAM to print nano-treated AA2024 and utilize porosity analysis as a measure of printing quality. Nanoparticle-altered microstructural features, including grain size, grain morphology, and secondary phase distribution, are analyzed. Then, by heat-treating the nano-treated

Departments of [1]Mechanical and Aerospace Engineering and [2]Materials Science and Engineering, University of California, Los Angeles, Los Angeles, California, USA.

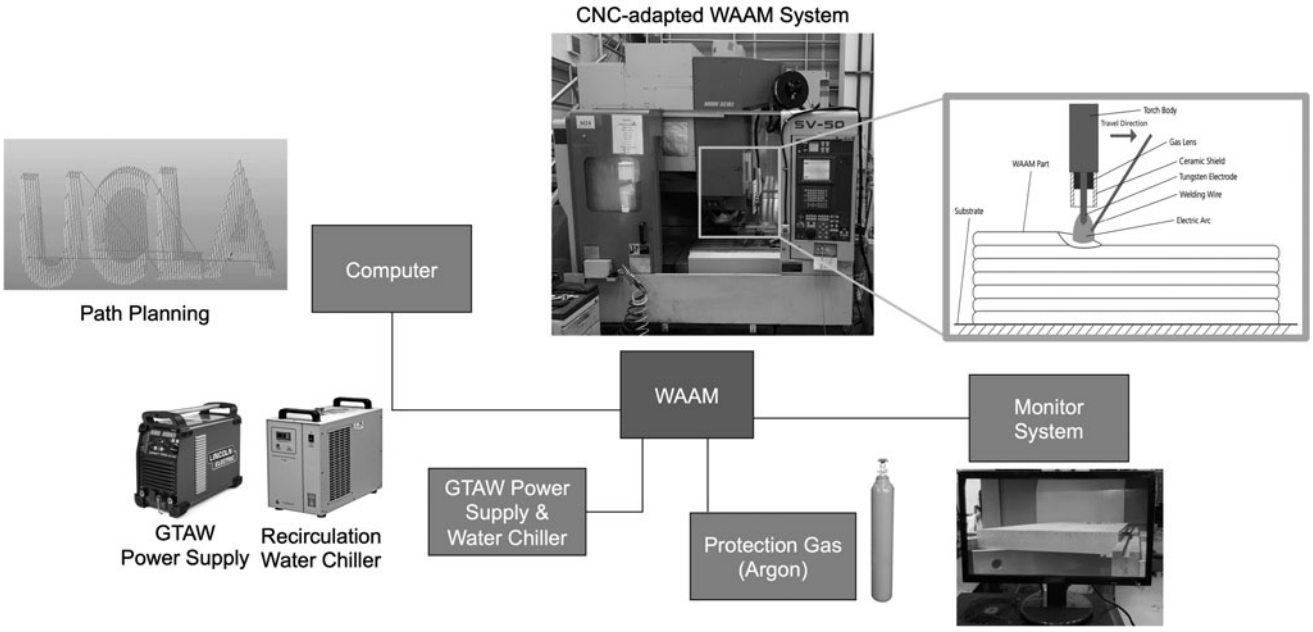

FIG. 1. Schematic of the CNC-adapted WAAM system. CNC, computer numerical control; WAAM, wire-arc additive manufacturing.

deposit, we observed a modified microstructure and further discuss the effect of nanoparticles on solutionizing. Finally, the mechanical performance of both as-built and heat-treated AA2024 deposits are evaluated in terms of microhardness and tensile testing and are compared with commercial wrought products.

Materials and Methods

WAAM materials and process

A gas–tungsten–arc-welding-based WAAM system was adapted on a Mori Seiki SV50 computer numerical control machine (as shown in Fig. 1). An electric arc powered by an AC power supply was generated at the tip of a nonconsumable tungsten electrode, while feedstock wire was fed from the side and deposited onto the AA 2024 substrate. The printing area was shielded by a steady supply of argon to prevent oxidation. The final three-dimensional geometry was printed line by line and layer by layer. The feedstock wire used was nano-treated AA2024 welding wire (1.2 mm in diameter from MetaLi, LLC.). By employing the printing parameters summarized in Table 1, a 10-layer block (13 mm height) was successfully printed. A modified T6 heat treatment was conducted with step solutionizing at 450°C for 1 h and 493°C for 1 h, followed by 12 h of aging at 190°C.

Table 1. Wire-Arc Additive Manufacturing Deposition Parameters Used for Fabrication of the Specimen

Mean wire feed rate, $\bar{v}_{WF}$, [m/min]	2.8
AC current, $\bar{I}$, [A]	150
Frequency, [Hz]	200
Electrode balance [%]	85
Mean voltage, $\bar{V}$, [V]	14
Travel speed, [mm/s]	4.2
Energy density, [kJ/mm]	0.5

Materials characterization

The chemical composition of the nano-treated AA2024 wire and its WAAM deposit (the deposit is also referred to as WAAM-AA2024 throughout the article) were characterized by inductively coupled plasma-mass spectrometry (ICP-MS; PerkinElmer NexION 2000), with three replicated measurements conducted with background correction. The phase compositions of AA 2024 deposits were characterized in X-ray diffraction (XRD) on Panalytical X'Pert Pro with 45 kV acceleration voltage. The scanning program was set to 20°–110° for scanning range, 0.05° for step size, and 1°/min for scanning speed.

Samples for microstructural characterization of the deposit were prepared by initial grinding on SiC papers (down to 1200 grit) and then further polishing using alumina suspensions of 1, 0.3, and 0.05 μm. The detailed microstructure of WAAM-AA2024 was revealed under scanning electron microscopy (SEM; ZEISS Supra 40VP) equipped with energy-dispersive spectroscopy (EDS). Grain boundaries were electrolytically etched using Barker's reagent and revealed under polarized light with an optical microscope. The grain size was further calculated in ImageJ using the standard linear intercept method outlined by American Society for Testing and Materials (ASTM).

Table 2. Chemical Compositions (wt.%) of the Nano-Treated AA2024 Wire and Wire-Arc Additive Manufacturing Deposit

	Al	*Cu*	*Mg*	*Ti*	*Fe*	*Mn*
Wire	Bal.	4.70	1.53	1.26	0.16	0.009
Deposit	Bal.	4.48	1.43	1.36	0.14	0.009

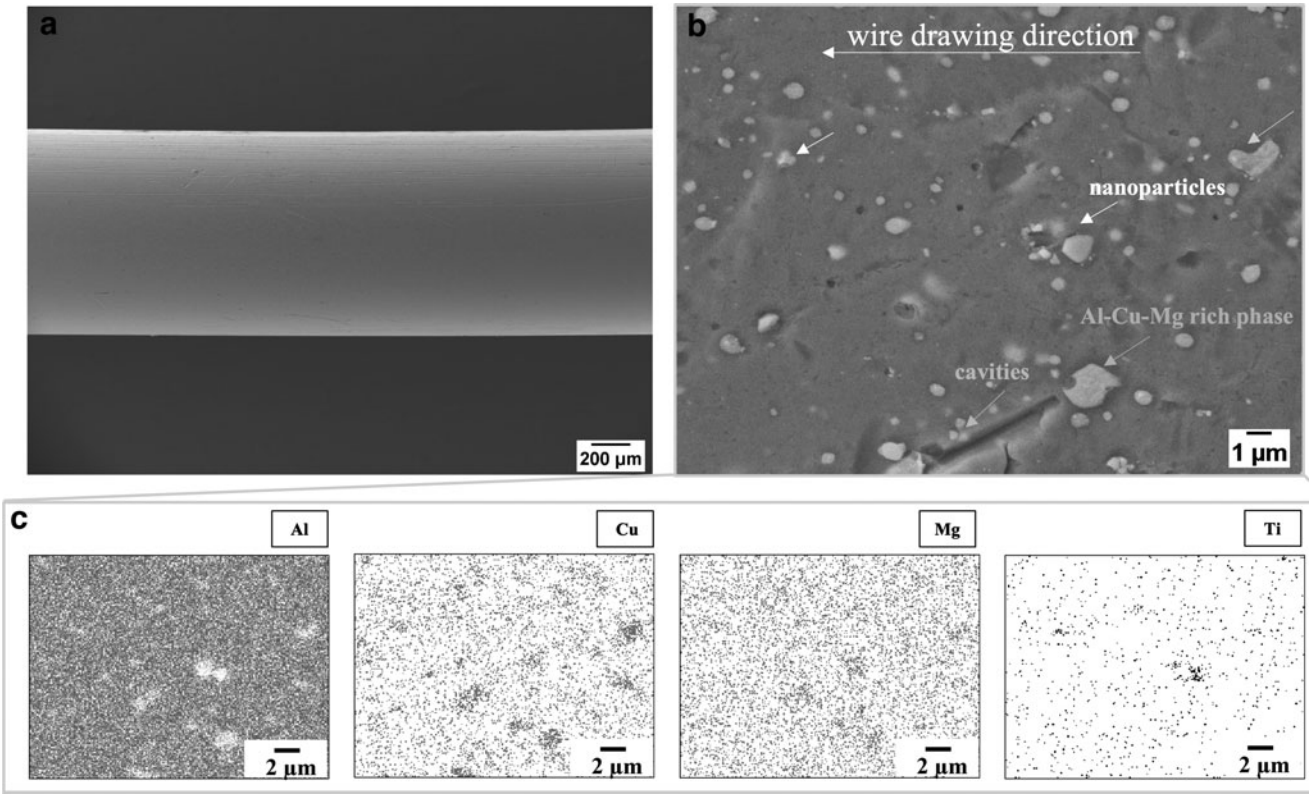

FIG. 2. SEM images of nano-treated AA2024 wire: **(a)** wire surface; **(b)** wire cross sections with **(c)** EDS mapping. EDS, energy-dispersive spectroscopy; SEM, scanning electron microscopy.

Mechanical performance was evaluated in terms of microhardness and tensile strength. Vickers microhardness measurements were collected on a LECO LM800AT tester using a load of 200 gf and a dwell time of 10 s. Two identical rows of indentations were created on each sample transversing 13 mm of the polished surface (Fig. 7). Both points at the same distance were averaged to yield a single point on the profile. One sample was tested for each condition (as-built and heat-treated).

Tensile bars were cut on an AgieCharmilles CUT 200 with wire electric discharge machining (EDM) before being tested on an Instron ElectroPuls E1000 mechanical tester at a strain rate of 0.001/s. Three tensile bars for each condition (as-built longitudinal direction, as-built transverse direction, heat-treated longitudinal direction, and heat-treated transverse direction) were prepared. All 12 tensile bars were gently ground before testing to remove surface inconsistencies resulting from the wire EDM process. After tensile testing, the fracture surfaces of the broken tensile bars were examined using SEM.

Results and Discussion

Chemical composition and microstructure

The alloying compositions of the novel nano-treated AA2024 wire and its deposition were quantified by ICP-MS and are summarized in Table 2. Owing to the high-

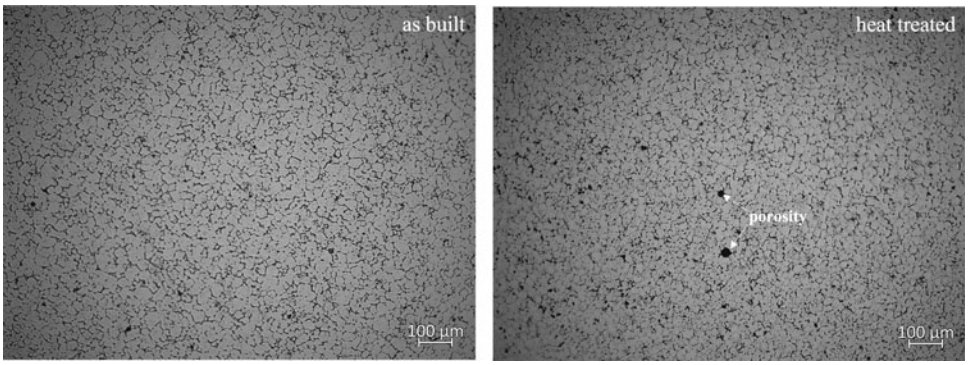

FIG. 3. Optical microstructures of etched cross sections for as-built and heat-treated samples.

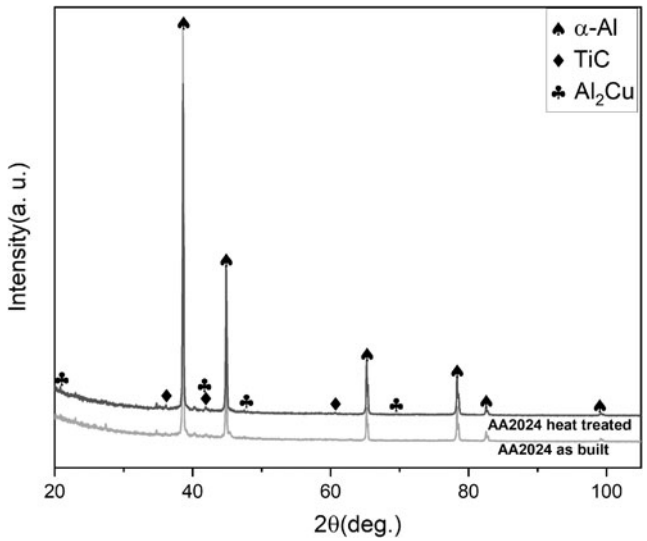

FIG. 4. XRD spectra of WAAM-AA2024 in as-built and heat-treated conditions. XRD, X-ray diffraction.

temperature deposition characteristics of WAAM, volatile elements such as Mg tend to evaporate.[17] In this study, we used a lower deposition power to maintain the designed alloy composition. As a result, only minor reductions of Mg and Cu were observed in the final deposit.

The surface of the nano-treated AA2024 wire was analyzed under SEM (Fig. 2a). The surface is smooth and clean, although with discernable scratches from the wire drawing process. Furthermore, the wire's cross section (Fig. 2b) with the Cu- and Mg-rich phases was identified using EDS mapping; Ti signals from the same area indicate well-dispersed TiC nanoparticles. Cavities are mainly found around hard secondary phases, which sometimes get detached from the matrix and leave shallow holes/porosities.[3]

The nano-treated AA2024 wire was successfully printed without any cracks using WAAM. Porosity levels and sizes within the deposit were analyzed in ImageJ, and the results suggest that good printing quality with a low porosity level was achieved. Porosity areal fraction was calculated at 0.19% with an average pore size of 9.4 μm. After etching, the grain boundaries for as-built and heat-treated cross sections were made visible (Fig. 3).

Instead of columnar grain structures that are commonly induced by solidification-associated thermal flow in conventional WAAM,[18,19] the nano-treated AA2024 deposit's cross section is dominated by fine equiaxed grain structures with an average size of 23.2 ± 0.4 μm (Fig. 3-as built). Nanoparticles promote heterogeneous nucleation[20–22] and refine grains during printing and also prevent grain growth during heat treatment. The heat-treated cross section has an average grain size of 25.6 ± 0.7 μm, with negligible coarsening compared with the as-built specimen; minor porosities are shown as black spots (Fig. 3-heat treated). It is believed that a homogenous microstructure will result in more isotropic material properties.

The XRD results of WAAM-AA2024 (Fig. 4) reveal the major phases in as-built and heat-treated conditions. TiC peaks in both spectra prove the presence of TiC nanoparticles after high-temperature deposition and their retention after heat treatment. The major strengthening phase, Al_2Cu, is also identified; Al_2Cu in as-built specimens is usually coarse and

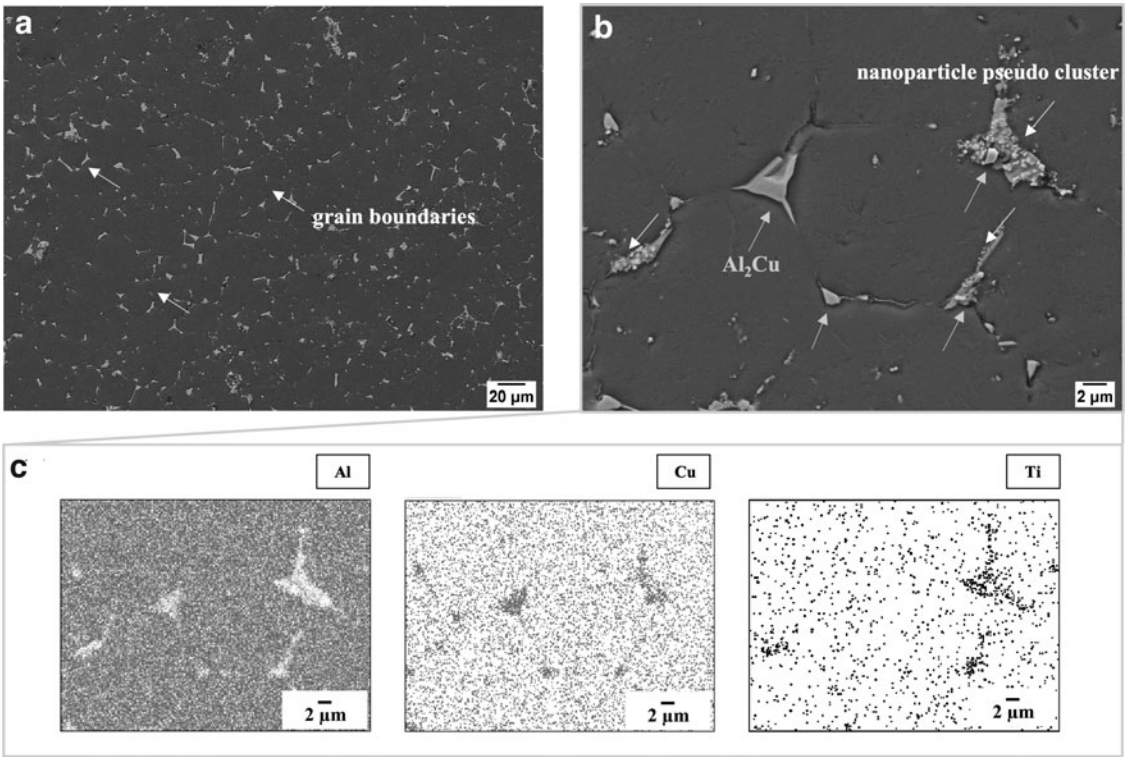

FIG. 5. SEM images of nano-treated AA2024 cross sections in as-built **(a, b)** conditions; **(c)** EDS mapping of **(b)**.

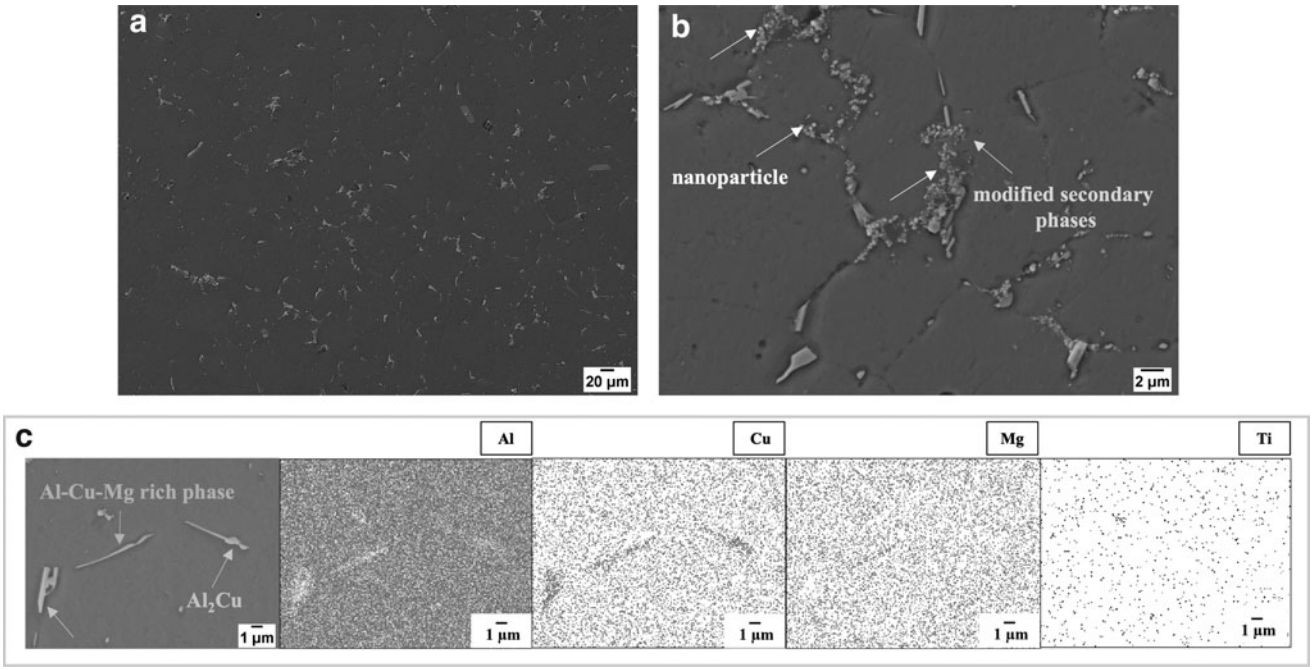

FIG. 6. SEM images of nano-treated AA2024 cross section in heat-treated **(a–c)** conditions; **(c)** EDS mapping.

bulky and forms on grain boundaries. During solute redistribution while undergoing heat treatment, it will fully dissolve and re-precipitate out uniformly and more finely throughout the matrix.

The cross sections of WAAM-AA2024 were analyzed using electron microscopy, and the results are highlighted (in Fig. 5). The secondary phases predominantly form on grain boundaries, especially at grain boundary junctions. Their morphologies, which are mainly triangular-shaped or match the shape of the junction, are different from those in the wire. These secondary phases are identified as Al_2Cu with high Cu and Al signals, as highlighted in the EDS maps. The Ti signal map indicates TiC nanoparticles in pseudo-clusters around secondary phases instead of random distributions, the latter as observed in the wire. A visual comparison between nanoparticles in the wire (Fig. 2) and those in the deposition confirms a lack of coarsening during the deposition process.

The microstructure of heat-treated WAAM-AA2024 is shown in Figure 6. The formerly coarse Al_2Cu phases were dissolved during solution treatment and re-precipitated more finely and uniformly after aging. The previously prevailing triangular-shaped morphology of the secondary phase is replaced by an acicular morphology, identified as Al_2Cu (Fig. 6c). TiC nanoparticles are mainly located around these acicular phases as shown in Figure. 6b, sometimes even fragmenting into smaller pieces. This phenomenon was also observed in as-built AA2024 cross sections in a previously published study.[6] The nanoparticle-modified secondary phase has the potential to improve liquid backfilling during the semisolid stage of solidification, which mitigates the hot cracking problem.[6,13] The nanoparticle in the Ti signal map suggests its size is still under control.

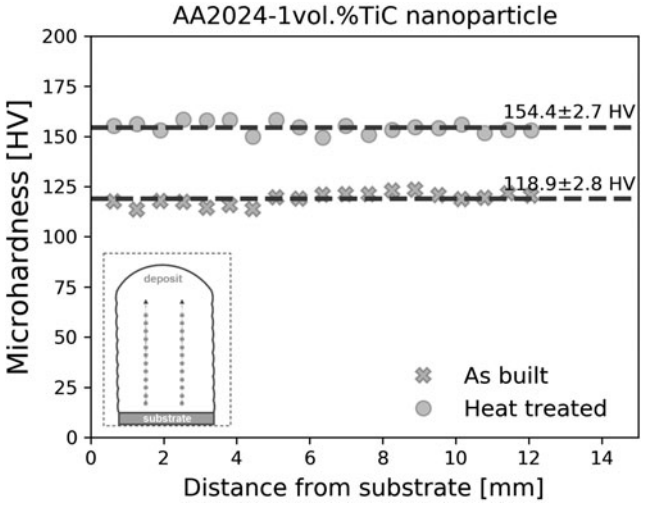

FIG. 7. Microhardness profiles along the building direction for as-built and heat-treated samples.

TABLE 3. SUMMARY OF TENSILE TEST RESULT

	Yield stress (MPa)	*Ultimate tensile stress (MPa)*	*Strain (%)*
As-built			
Longitudinal	166 ± 11	328 ± 10	8.0 ± 2.2
Transverse	178 ± 1	304 ± 6	7.4 ± 1.5
Heat-treated (T6)			
Longitudinal	324 ± 5	428 ± 5	7.4 ± 0.1
Transverse	303 ± 28	403 ± 5	7.4 ± 0.3
T6			
Wrought[23]	345	427	5

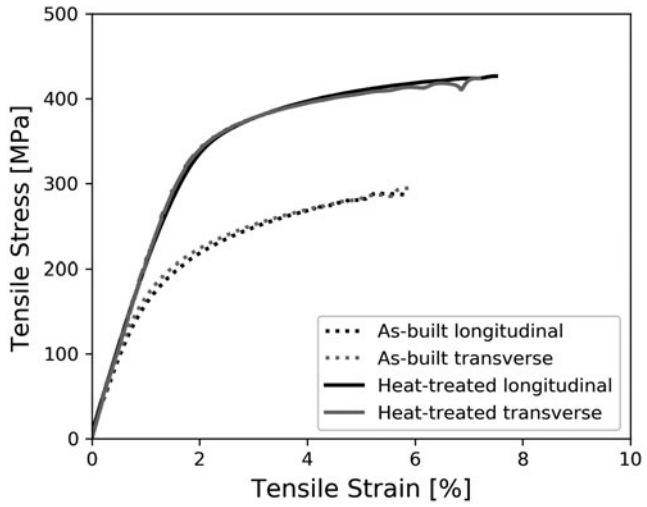

FIG. 8. Engineering stress–strain curves for nano-treated AA2024 deposits.

Mechanical properties

Owing to the intrinsic thermal conditions present during deposition, the maximum thermal gradient is aligned with the building direction, which promotes the growth of columnar grains. This columnar texture will engender anisotropic mechanical performance and further limit application potential. To confirm that nanoparticles eliminated this behavior, we measured the microhardness of the AA2024 sample along its building direction (Fig. 7).

In the as-built condition, the microhardness profile has minor fluctuations, and the average value is 118.9 ± 2.8 HV. After heat treatment, the microhardness values remain stable along the building direction with an average value of 154.5 HV, which exceeds the microhardness of wrought AA2024 (142 HV).[23] Thus, the microhardness profile shows consistent results with the observations we made in Figure 3, where TiC nanoparticles successfully eliminated the formation of columnar grains and reduced grain coarsening during heat treatment. The results suggest the microhardness of the nano-treated AA2024 has uniform mechanical properties despite the unidirectional thermal flow along the building direction.

Tensile testing was performed to evaluate mechanical properties in the longitudinal and transverse directions. The results in Table 3 suggest the ultimate tensile stress and strain can reach up to 328 MPa and 8% as built. After heat treatment, with a more uniform distribution of Al_2Cu, the ultimate tensile stress increases by >100 MPa in both directions, whereas strain remains at 7.4%. The engineering stress–strain curves (Fig. 8) suggest isotropic tensile properties in nano-treated AA2024 deposits. The nanoparticle-induced microstructure solved the anisotropic mechanical performance challenge in the conventional WAAM process. In addition, the tensile strength of nano-treated AA2024 is comparable with that of commercial AA2024-T6, while the ductility is superior.

Fracture surfaces

The fracture surfaces of heat-treated AA2024 tensile bars were further characterized using SEM, and the results are shown in Figure 9. The fracture surfaces in the longitudinal direction (Fig. 9a) and transverse direction (Fig. 9c) show similar morphologies. At lower magnification,

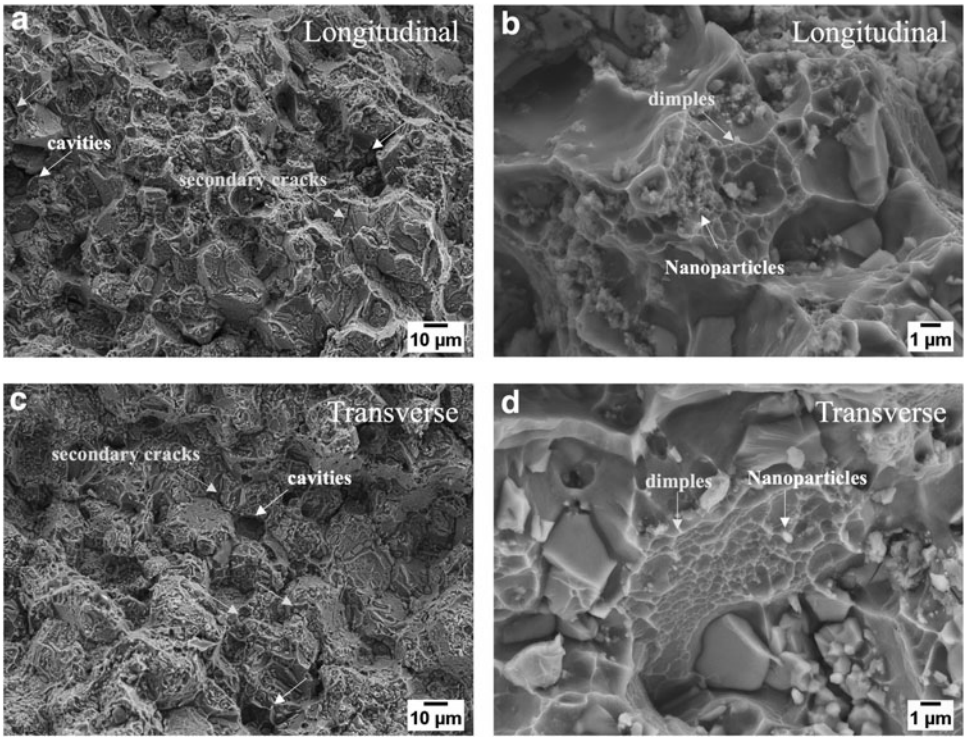

FIG. 9. Fractography of the nano-treated AA2024 deposits in both longitudinal **(a, b)** and transverse **(c, d)** directions.

a polyhedron-like fracture is observed, and the visible cavities are due to secondary phase detachment and porosity. Furthermore, some secondary cracks with transgranular fracture paths are found around those cavities, which compromised the material's ductility. At high magnification, as shown in Figure 9b and d, fine and shallow dimple-like fracture surfaces appear in both the longitudinal and transverse directions. Nanoparticle pseudo-clusters were also observed at grain boundaries.

Conclusions

This study uses nano-treated AA2024 wire as feedstock in WAAM to demonstrate the successful printing of hot-crack-sensitive high-performance aluminum alloy AA2024. Nano-treatment within the deposit shows excellent results in eliminating solidification defects and refining grain structures. The following conclusions can be drawn based on the microstructural analysis and mechanical testing in as-built and heat-treated conditions:

- TiC nanoparticles improve the printability of AA2024 with respect to the absence of cracks and low porosity levels.
- TiC nanoparticles inhibit columnar grain growth and promote heterogeneous nucleation. The resulting microstructure contains fine and equiaxed grains with an average size of $\sim 23.2\,\mu$m throughout the deposition. During cyclic thermal exposure and heat treatment, there is no significant grain coarsening.
- Uniform microhardness and isotropic tensile stress are well correlated to the homogenous microstructure that was observed. The deposit's mechanical performance is further enhanced with precipitation strengthening from Al_2Cu after heat treatment. The resulting microhardness, tensile strength, and elongation reach up to 154.4 HV, 428 MPa, and 7.4%, which are competitive with its commercial wrought counterpart.
- After heat treatment, fracture surfaces in the longitudinal and transverse directions share similarly ductile morphologies with fine shallow dimple-like structures.

Acknowledgments

The authors are thankful to MetaLi, LLC for providing the nano-treated AA2024 wire. The authors are also thankful to Yuxin Zeng for insightful discussions in this study.

Authors' Contributions

Investigation, formal analysis, methodology, and writing—original draft by Y.C.; investigation and writing—reviewing and editing by N.M.; methodology and formal analysis by T.Z; methodology by J.L.; formal analysis, writing—review and editing, and project administration by X.L.

Author Disclosure Statement

No competing financial interests exist.

Funding Information

No funding was received for this article.

References

1. Shabestari SG, Ghoncheh MH. Investigation on the effect of cooling rate on hot tearing susceptibility of Al2024 alloy using thermal analysis. Metall Mater Trans B 2015; 46(6):2438–2448; doi: 10.1007/s11663-015-0450-7.
2. Nie X, Zhang H, Zhu H, et al. Analysis of processing parameters and characteristics of selective laser melted high strength Al-Cu-Mg alloys: From single tracks to cubic samples. J Mater Process Technol 2018;34(11):69–77; doi: 10.1016/j.jmatprotec.2018.01.030.
3. Klein T, Arnoldt A, Lahnsteiner R, et al. Microstructure and mechanical properties of a structurally refined Al–Mg–Si alloy for wire-arc additive manufacturing. Mater Sci Eng A 2022;830:142318; doi: 10.1016/j.msea.2021.142318.
4. Opprecht M, Garandet J-P, Roux G, et al. A solution to the hot cracking problem for aluminium alloys manufactured by laser beam melting. Acta Mater 2020;197:40–53; doi: 10.1016/j.actamat.2020.07.015.
5. Martin JH, Yahata BD, Hundley JM, et al. 3D printing of high-strength aluminium alloys. Nature 2017;549(7672): 365–369; doi: 10.1038/nature23894.
6. Sokoluk M, Cao C, Pan S, et al. Nanoparticle-enabled phase control for arc welding of unweldable aluminum alloy 7075. Nat Commun 2019;10(1):98; doi: 10.1038/s41467-018-07989-y.
7. Tang Z, Vollertsen F. Influence of grain refinement on hot cracking in laser welding of aluminum. Weld World 2014;58(3):355–366; doi: 10.1007/s40194-014-0121-3.
8. Hagenlocher C, Weller D, Weber R, et al. Reduction of the hot cracking susceptibility of laser beam welds in AlMgSi alloys by increasing the number of grain boundaries. Sci Technol Weld Join 2019;24(4):313–319; doi: 10.1080/13621718.2018.1534775.
9. Nie X, Zhang H, Zhu H, et al. Effect of Zr content on formability, microstructure and mechanical properties of selective laser melted Zr modified Al-4.24Cu-1.97Mg-0.56Mn alloys. J Alloys Compd 2018;764:977–986; doi: 10.1016/j.jallcom.2018.06.032.
10. Zhang H, Zhu H, Nie X, et al. Effect of zirconium addition on crack, microstructure and mechanical behavior of selective laser melted Al-Cu-Mg alloy. Scr Mater 2017;134:6–10; doi: 10.1016/j.scriptamat.2017.02.036.
11. Wang P, Gammer C, Brenne F, et al. Microstructure and mechanical properties of a heat-treatable Al-3.5Cu-1.5Mg-1Si alloy produced by selective laser melting. Mater Sci Eng A 2018;711:562–570; doi: 10.1016/j.msea.2017.11.063.
12. Cao C, Yao G, Jiang L, et al. Bulk ultrafine grained/nanocrystalline metals via slow cooling. Sci Adv 2019;5(8) :eaaw2398; doi: 10.1126/sciadv.aaw2398.
13. Sokoluk M, Yuan J, Pan S, et al. Nanoparticles enabled mechanism for hot cracking elimination in aluminum alloys. Metall Mater Trans A 2021;52(7):3083–3096; doi: 10.1007/s11661-021-06302-9.
14. Pan S, Wang T, Jin K, et al. Understanding and designing metal matrix nanocomposites with high electrical conductivity: A review. J Mater Sci 2022;57(12):6487–6523; doi: 10.1007/s10853-022-07010-4.
15. Pan S, Yuan J, Zheng T, et al. Interfacial thermal conductance of in situ aluminum-matrix nanocomposites. J Mater Sci 2021;56(24):13646–13658; doi: 10.1007/s10853-021-06176-7.
16. Pan S, Jin K, Wang T, et al. Metal matrix nanocomposites in tribology: Manufacturing, performance, and mechanisms. Friction 2022; doi: 10.1007/s40544-021-0572-7.

17. Morais PJ, Gomes B, Santos P, et al. Characterisation of a high-performance Al–Zn–Mg–Cu alloy designed for wire arc additive manufacturing. Materials 2020;13(7):1610; doi: 10.3390/ma13071610.
18. Kok Y, Tan XP, Wang P, et al. Anisotropy and heterogeneity of microstructure and mechanical properties in metal additive manufacturing: A critical review. Mater Des 2018;139:565–586; doi: 10.1016/j.matdes.2017.11.021.
19. Baufeld B, van der Biest O. Mechanical properties of Ti-6Al-4V specimens produced by shaped metal deposition. Sci Technol Adv Mater 2009;10(1):015008; doi: 10.1088/1468-6996/10/1/015008.
20. Jia Y, Wang S, Shu D. Grain size prediction and investigation of 7055 aluminum alloy inoculated by Al–5Ti–1B master alloy. J Alloys Compd 2020;821:153504; doi: 10.1016/j.jallcom.2019.153504.
21. Greer AL, Bunn AM, Tronche A, et al. Modelling of inoculation of metallic melts: Application to grain refinement of aluminium by Al–Ti–B. Acta Mater 2000;48(11):2823–2835; doi: 10.1016/S1359-6454(00)00094-X.
22. Li J, Hage FS, Ramasse QM, et al. The nucleation sequence of α-Al on TiB2 particles in Al-Cu alloys. Acta Mater 2021;206:116652; doi: 10.1016/j.actamat.2021.116652.
23. Anonymous. Aluminum 2024-T6. n.d. Available from: https://www.matweb.com/search/DataSheet.aspx?MatGUID=ecf8530875cb4ded9675b827f77bfac5&ckck=1 [Last accessed: May 14, 2022].

Address correspondence to:
Xiaochun Li
Department of Mechanical and Aerospace Engineering
University of California, Los Angeles
Los Angeles, CA 90095
USA

E-mail: xcli@seas.ucla.edu